Journal of Geophysical Research: Oceans

RESEARCH ARTICLE
10.1029/2018JC013755

Special Section:
Oceanic Responses and Feedbacks to Tropical Cyclones

Tropical Cyclone Boundary Layer Rolls in Synthetic Aperture Radar Imagery

Lanqing Huang[1], Xiaofeng Li[2], Bin Liu[1], Jun A. Zhang[3], Dongliang Shen[4], Zenghui Zhang[1], and Wenxian Yu[1]

[1]Shanghai Key Laboratory of Intelligent Sensing and Recognition, Shanghai Jiao Tong University, Shanghai, China, [2]GST, National Oceanic and Atmospheric Administration/Satellite and Information Service, College Park, MD, USA, [3]National Oceanic and Atmospheric Administration/Atlantic Oceanographic and Meteorological Laboratory, Hurricane Research Division, Cooperative Institute for Marine and Atmospheric Studies, University of Miami, Miami, FL, USA, [4]College of Marine Sciences, Shanghai Ocean University, Shanghai, China

Abstract Marine atmospheric boundary layer (MABL) roll plays an important role in the turbulent exchange of momentum, sensible heat, and moisture throughout MABL of tropical cyclone (TC). Hence, rolls are believed to be closely related to TC's development, intensification, and decay processes. Spaceborne synthetic aperture radar (SAR) provides a unique capability to image the sea surface imprints of quasi-linear streaks induced by the MABL rolls within a TC. In this study, sixteen SAR images, including three images acquired during three major hurricanes: Irma, Jose, and Maria in the 2017 Atlantic hurricane season, were utilized to systematically map the distribution and wavelength of MABL rolls under the wide range of TC intensities. The images were acquired by SAR onboard RADARSAT-1/2, ENVISAT, and SENTINEL-1 satellites. Our findings are in agreement with the previous one case study of Hurricane Katrina (2005), showing the roll wavelengths are between 600 and 1,600 m. We also find that there exist roll imprints in eyewall and rainbands, although the boundary layer heights are shallower there. Besides, the spatial distribution of roll wavelengths is asymmetrical. The roll wavelengths are found to be the shortest around the storm center, increase and then decrease with distance from storm center, reaching the peak values in the range of d^*-2d^*, where d^* is defined as the physical location to TC centers normalized by the radius of maximum wind. These MABL roll characteristics cannot be derived using conventional aircraft and land-based Doppler radar observations.

Key Points:
- Tropical cyclone boundary layer rolls leave linear streaks on the ocean surface that are imaged by synthetic aperture radar (SAR)
- SAR images are analyzed to systematically map the distribution and wavelength of boundary layer rolls under different storm conditions
- The roll wavelengths are found to be the shortest around the storm center, increase and then decrease with distance from storm center

Correspondence to:
X. Li,
Xiaofeng.Li@noaa.gov

Citation:
Huang, L., Li, X., Liu, B., Zhang, J. A., Shen, D., Zhang, Z., & Yu, W. (2018). Tropical cyclone boundary layer rolls in synthetic aperture radar imagery. *Journal of Geophysical Research: Oceans*, *123*, 2981–2996. https://doi.org/10.1029/2018JC013755

Received 5 JAN 2018
Accepted 31 MAR 2018
Accepted article online 6 APR 2018
Published online 26 APR 2018

1. Introduction

Tropical cyclone (TC) is one of the overwhelmingly natural catastrophes which could cause devastating effects on human population such as loss of life and property (Goldenberg et al., 2001; Pielke & Landsea, 1998). There are some multiscale wind features which contribute to the TC's damage during landfalls (Zhang & Li, 2017). Among these features, the marine atmospheric boundary layer (MABL) roll plays an important role in the turbulent exchange of momentum, sensible heat, and moisture throughout the boundary layer of TC's (Zhang et al., 2008). Therefore, rolls are believed to be closely related to storm development and intensification (Zhang et al., 2011). Overland and Wilson (1984) estimated the mesoscale variability in marine winds at midlatitude and also suggested that enhanced vertical flux in the oceanic mixed layer occurs at length scales of atmospheric boundary layer structures. Since dynamically rolls impact the vertical turbulent fluxes that are crucial to hurricane forecast model physics, the MABL roll characteristics and their locations relative to the maximum wind will be invaluable information to help evaluate the hurricane models.

For decades, researchers have been investigating rolls in the boundary layer via analyzing data from Doppler radar and aircraft dropsonde. Recently, a relatively new satellite remote sensing tool, synthetic aperture radar (SAR), has also been utilized to study the MABL rolls. Besides, Foster (2005) has developed a theory for rolls and indicated that TC boundary is a favorable environment for roll formation.

From mobile Doppler radar, Wurman and Winslow (Wurman & Winslow, 1998) observed the subkilometer-scale rolls in the boundary layer of Category 3 hurricane Fran (1996). Then, via National Weather Service WSR-88D Doppler radars, Morrison et al. (2005) indicate that rolls occur in 35–69% of the radar volumes,

with a typical wavelength of 1,450 m. Later, Lorsolo et al. (2008) analyzed rolls of Category 5 Hurricanes Isabel (2003) and Category 4 Frances (2004) by Shared Mobile Atmosphere Research and Teaching (SMART) radars. They found that the majority of wavelength of rolls are between 200 and 650 m, which is consistent with the study of Wurman and Winslow (Wurman & Winslow, 1998).

Rolls have also been studied by aircraft data by following the methodology proposed by Zhang et al. (2008). Their analyses of airborne data suggest that roll vortices may be a significant factor modulating the air-sea momentum exchange. Recently, Svensson et al. (2017) presented results concerning roll persistence during situations with advection to a strongly stratified boundary layer via SAR and aircraft data. Gao et al. (2017) studied the impact of rolls on the intensification process of the TC's and identified a pathway by which rolls can affect the structure and the intensification of the simulated TC's.

SAR can be utilized in observing MABL rolls in day-night conditions, resulting from the high resolution ($<$100 m) and capability of penetrating clouds (Katsaros et al., 2000, 2002; Li et al., 2013a, 2013b; Reppucci et al., 2006; Zhang & Li, 2017). SAR measures the ocean surface roughness by the physical value named normalized radar cross section (NRCS) and provides a unique capability to image the sea surface imprints of quasi-linear streaks induced by the MABL rolls within a TC. Therefore, SAR is regarded as a useful tool for roll quantitative study (Li et al., 2013b). Katsaros et al. (2000, 2002) found roll features in the regions between the rainbands of hurricanes in RADARSAT-1 SAR images. Reppucci et al. (2006) analyzed the roll wavelength of Hurricane Katrina using the Fast Fourier Transform (FFT) algorithm. Zhang and Li (2017) retrieved roll characteristics for Hurricane Isidore and Typhoon Fitow from SAR images, indicating these SAR-derived characteristics are in agreement with that from Doppler radar data. They also showed that the rolls are generally aligned in wind direction.

Due to the three major hurricanes: Harvey, Irma, and Maria, with total cost over $316.51 billion (USD), 2017 Atlantic hurricane season becomes the most disastrous season on record (Wikipedia, the free encyclopedia, 2017). Therefore, predicting the potential damage of these destructive TC's and taking effective precautions is necessary. In this paper, we elaborate the roll characteristics from SAR images and demonstrate the new capabilities to use SAR data for MABL roll research. Note that we use SAR images for roll analyses for two reasons: (1) the rolls are possibly prevalent in TC conditions (Foster, 2005); (2) and some sporadic case studies (Li et al., 2013a, 2013b; Reppucci et al., 2006) shed light on the potential of quantitative analyses of SAR-derived information for the MABL roll research.

In this study, we collected sixteen SAR images acquired for eight TC's (2005 Hurricane Katrina, 2010 Hurricane Earl, 2010 Typhoon Malakas, 2010 Typhoon Megi, 2010 Typhoon Fanapi, 2017 Hurricane Irma, 2017 Hurricane Jose, and 2017 Hurricane Maria). We collected these SAR images for two reasons: (1) SAR images which can be colocated with the stepped frequency microwave radiometer (SFMR) data are collected as far as possible; (2) SAR images under different-scale storm conditions are collected so as to guarantee the general results. The MABL roll characteristics are retrieved from SAR images via the FFT algorithm. We analyze the frequency of roll occurrence and quantify the wavelength distribution. The variations of roll wavelengths associated with locations relative to the storm center are quantitatively discussed. The meaning of this work is threefold. First, we demonstrate that SAR allows us to systematically map the distribution and wavelength of MABL rolls under different-scale hurricane conditions for the first time. Additionally, we present the MABL roll characteristics and its spatial variation with respect to TC center. Furthermore, since rolls are shown to be closely related to hurricane dynamics, we expect this work to be promising to bring roll-induced effects into hurricane forecasting model.

The remainder of this paper is organized as follows. Section 2 describes the data set and the processing method. The results of SAR-derived roll characteristics are presented in section 3. In section 3, we discuss the occurrence of rolls, the relationships between roll wavelengths and distances with respect to storm center. Finally, the conclusions are drawn in section 4.

2. Data and Processing

2.1. SAR Data

In this paper, sixteen SAR images of eight TC's are used for roll analyses. Four of them are C-band RADARSAT-2 ScanSAR wide mode images covering four TC's acquired by the Canadian Space Agency (CSA) in

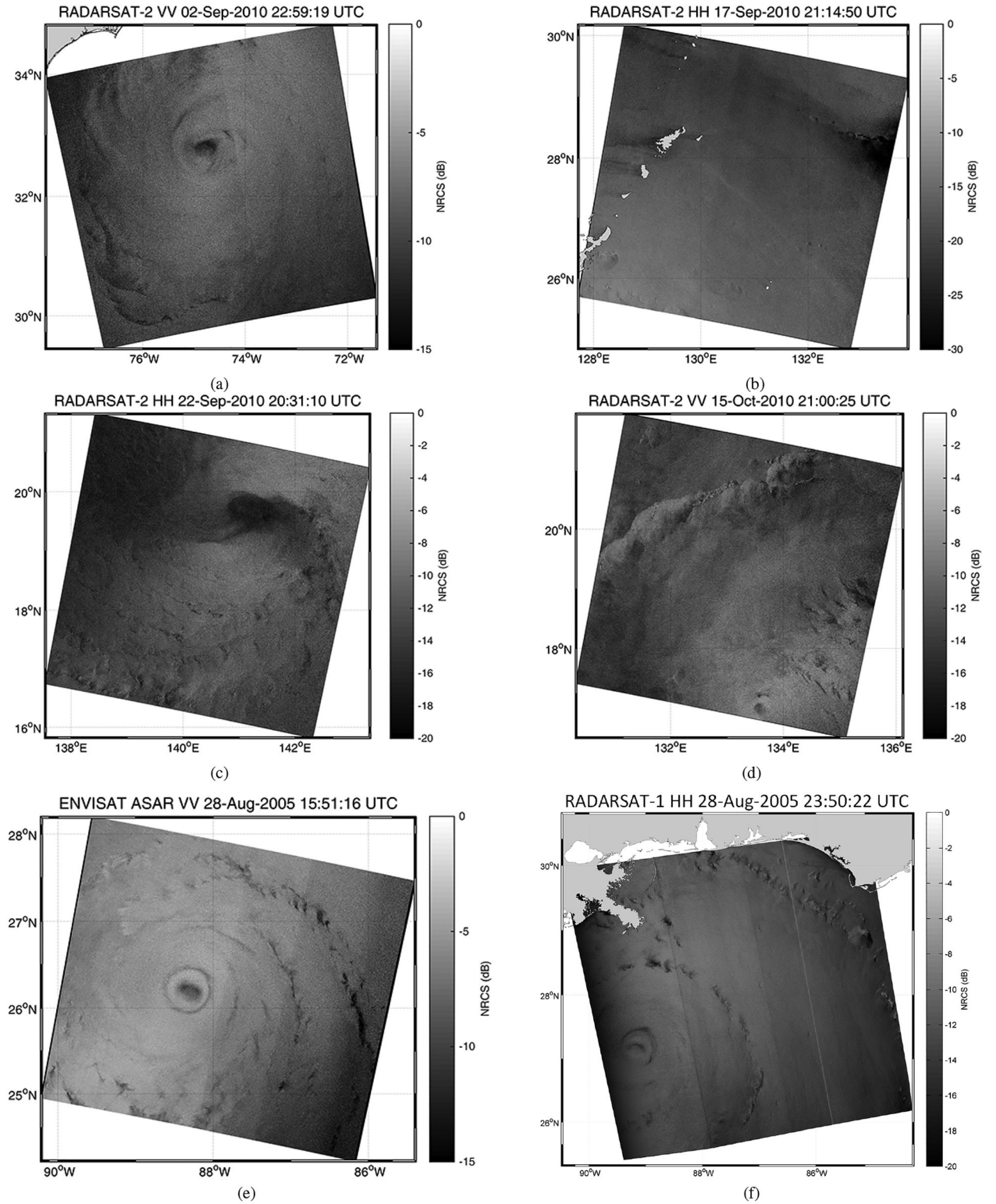

Figure 1. SAR images of various TC's. (a) Hurricane Earl 2010 by RADARSAT-2. (b) Typhoon Fanapi 2010 by RADARSAT-2. (c) Typhoon Malakas 2010 by RADARSAT-2. (d) Typhoon Megi 2010 by RADARSAT-2. (e) Hurricane Katrina 2005 by ENVISAT. (f) Hurricane Katrina 2005 by RADARSAT-1.

2010. Two C-band SAR images over Hurricane Katrina 2005, are acquired by Advanced Synthetic Aperture Radar (ASAR) ScanSAR wide mode and RADARSAT-1 ScanSAR wide mode, respectively. The SAR images covering the centers or the periphery of the eye locations are illustrated in Figure 1.

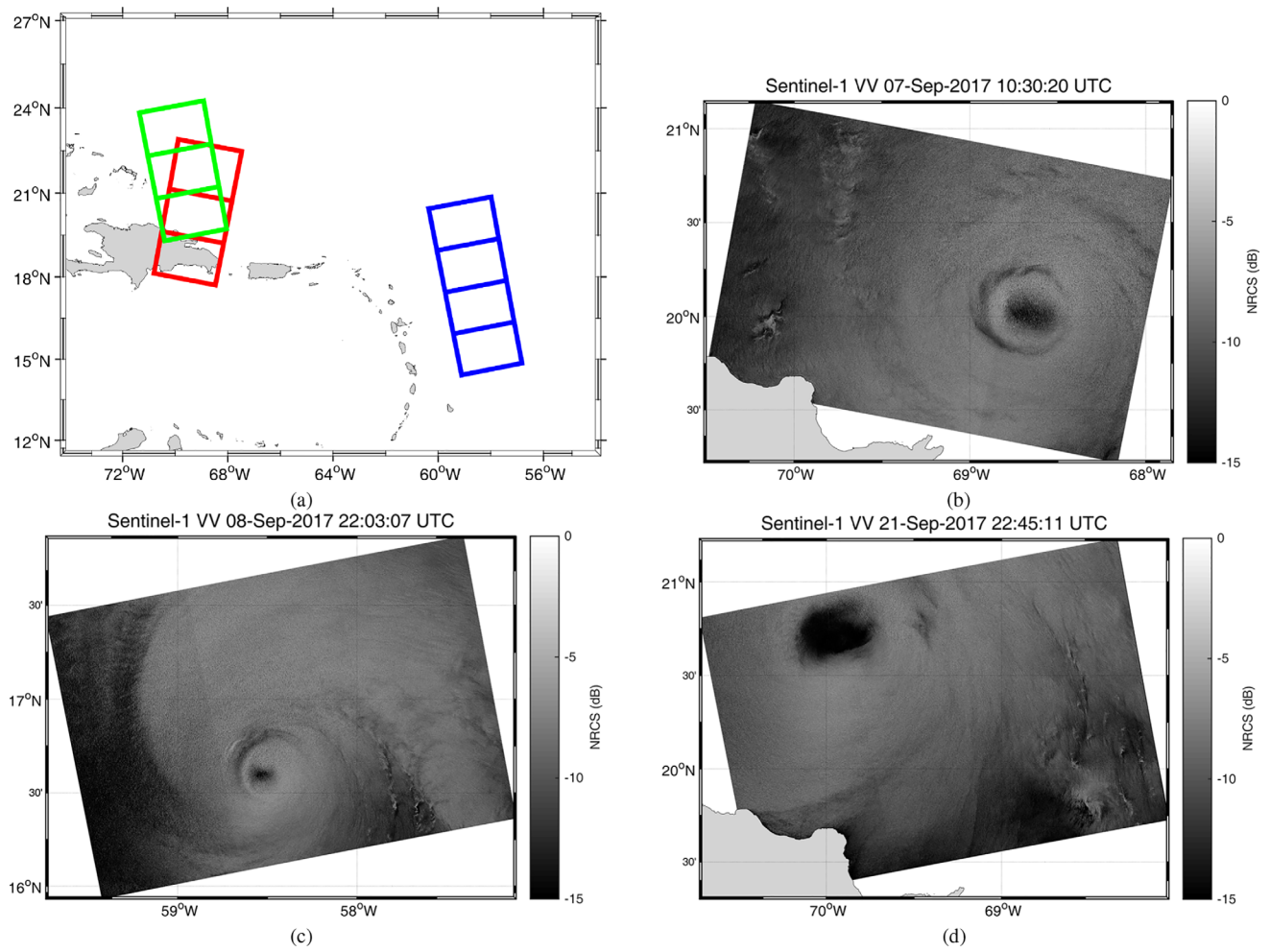

Figure 2. SENTINEL-1 SAR images of TC's. (a) Footprints of Hurricane Irma (red rectangles), Hurricane Jose (blue rectangles), and Hurricane Maria (green rectangles). (b) Hurricane Irma. (d) Hurricane Jose. (c) Hurricane Maria.

As for 2017 Atlantic hurricane, Hurricane Irma, Jose, and Maria are exactly captured by SENTINEL-1A IW mode. Hurricane Irma, recorded as Category 5 intensity, was captured at near the Dominican Republic. Hurricane Jose was captured when it is a Category 4 hurricane in the open ocean. Hurricane Maria was acquired between the Cockburn Town and Dominican Republic as Category 3. Since the swath of SENTINEL-1 IW mode is 250 km, three or four images acquired just in seconds difference are combined to achieve wider

Table 1
Information of SAR Images of the Six TC's

Tropical cyclones	Date/time (UTC)	Satellite	Polarization	Swath (km)	Image number	Storm center (lat,lon)	Hemisphere for location of storm center	Category
Earl	2 Sep 2010 22:59	RADARSAT-2	VV/VH	500	1	(32.779°, −74.802°)	North	Category 3
Fanapi	17 Sep 2010 21:14	RADARSAT-2	HH/HV	500	1	(23.434°, 126.597°)	North	Category 2
Malakas	22 Sep 2010 20:31	RADARSAT-2	HH/HV	500	1	(19.566°, 141.436°)	North	Severe tropical storm
Megi	15 Oct 2010 21:00	RADARSAT-2	VV	500	1	(16.985°, 133.575°)	North	Category 1
Katrina	28 Aug 2005 15:51	ENVISAT	VV	400	1	(26.187°, −88.215°)	North	Category 5
Katrina	28 Aug 2005 23:50	RADARSAT-1	VV	500	1	(27.162°, −89.228°)	North	Category 5
Irma	7 Sep 2017 10:30	SENTINEL-1A	VV/VH	250	3	(20.050°, −68.650°)	North	Category 5
Jose	8 Sep 2017 22:03	SENTINEL-1A	VV/VH	250	4	(16.635°, −58.475°)	North	Category 4
Maria	21 Sep 2017 22:45	SENTINEL-1A	VV/VH	250	3	(20.858°, −69.917°)	North	Category 3

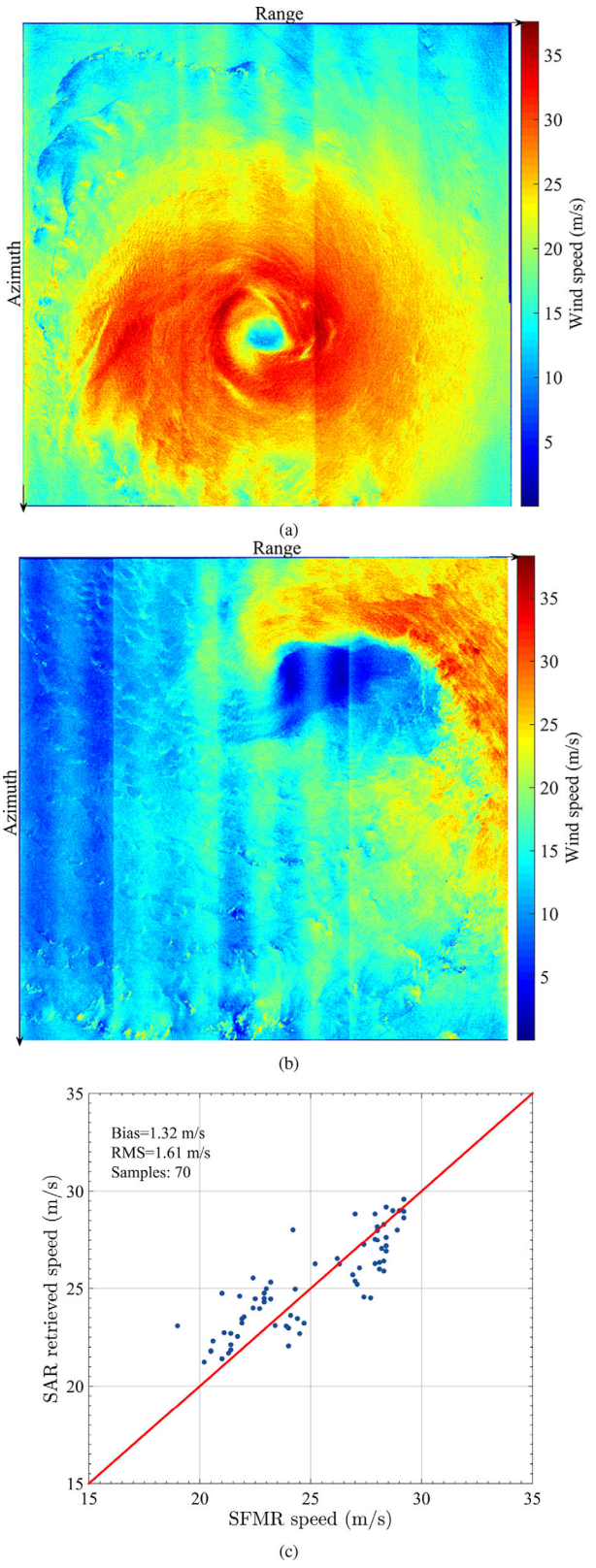

Figure 3. Wind speed retrievals by C-3PO. (a) Hurricane Earl. (b) Typhoon Malakas. (c) Comparison of retrieved wind speeds with collocated SFMR measurements.

coverage of hurricane. SAR images covering the centers or the periphery of the eye locations are illustrated in Figure 2.

The detailed information of the SAR images as well as the intensities of each storm on the Saffir-Simpson (SS) scale are given in Table 1.

2.2. Auxiliary Data

The best track (BT) data are provided by the National Oceanic and Atmospheric and Administration (NOAA) (http://www.nhc.noaa.gov/data/#hurdat). Since the TC was continuously moving, the precise position of the storm center at the acquisition time is difficult to determine. Here, we determine the position of storm center from BT data by linear interpolation between two closest BT locations (Zhang et al., 2017a). The calculated latitudes and longitudes of the six storm centers are shown in Table 1.

SAR images provide deep knowledge of the characteristics of sea surface wind fields with high spatial resolution and large spatial coverage and are widely used in TC monitoring (Friedman & Li, 2000; Jin et al., 2014, 2017; Li, 2015; Li et al., 2002; Lee et al., 2016; Zheng et al., 2016; Zhou et al., 2013). In extreme TC condition, the VH/HV polarization of SAR images can be utilized to observe the sea surface wind field by empirical models (Hwang et al., 2010; Shen et al., 2014; Shao et al., 2017; Zhang et al., 2012, 2017a, 2017b). This overcomes the SAR HH/VV signal saturation issues commonly encountered in SAR ocean surface wind retrievals. Here, the wind fields of TC are retrieved from RADARSAT-2 SAR images via the C-3PO geophysical model function (Zhang et al., 2017a). The results of wind field retrieval from SAR images are shown in Figure 3. These wind speed data will be used to analyze the correlation between wind speeds and rolls in section 3.2. Here, only the two RADARSAT-2 data, which have VH/HV data and captured TC centers are processed for two reasons. For one thing, the RADARSAT-1 and ENVISAT images do not provide HV/VH data. For another, due to the relatively low signal-to-noise ratio of SENTINEL-1 VH product, accurate wind speed retrieval is still an open question.

The stepped frequency microwave radiometer data (SFMR), on board the NOAA WP-3D and U.S. Air Force research aircraft, provide operational sea surface wind measurements under extreme conditions. In order to demonstrate the accuracy of SAR-retrieved wind fields, we collocate the retrieved data with the data obtained from the SFMR. As shown in Figure 3c, the 70 collocated data from Hurricane Earl are analyzed. The mean speed error is 1.3 m/s and the root mean square of estimation is 1.6 m/s, which demonstrate the availability and accuracy of SAR-retrieved wind speeds.

2.3. Extraction of Roll Characteristics

On the SAR images, the quasi-periodic streaks are visible on the sea surface, shown in Boxes A and B in Figure 4a. The brush-like features are interpreted as the imprints of the boundary layer rolls, since rolls modulate the sea surface roughness on the centimeter scale and change the Bragg wave spectrum (Li et al., 2013b; Zhang et al., 2008). The wavelengths of rolls range from subkilometer scales to around 2 km scales, and the directions of rolls are aligned with wind directions (Reppucci et al., 2006).

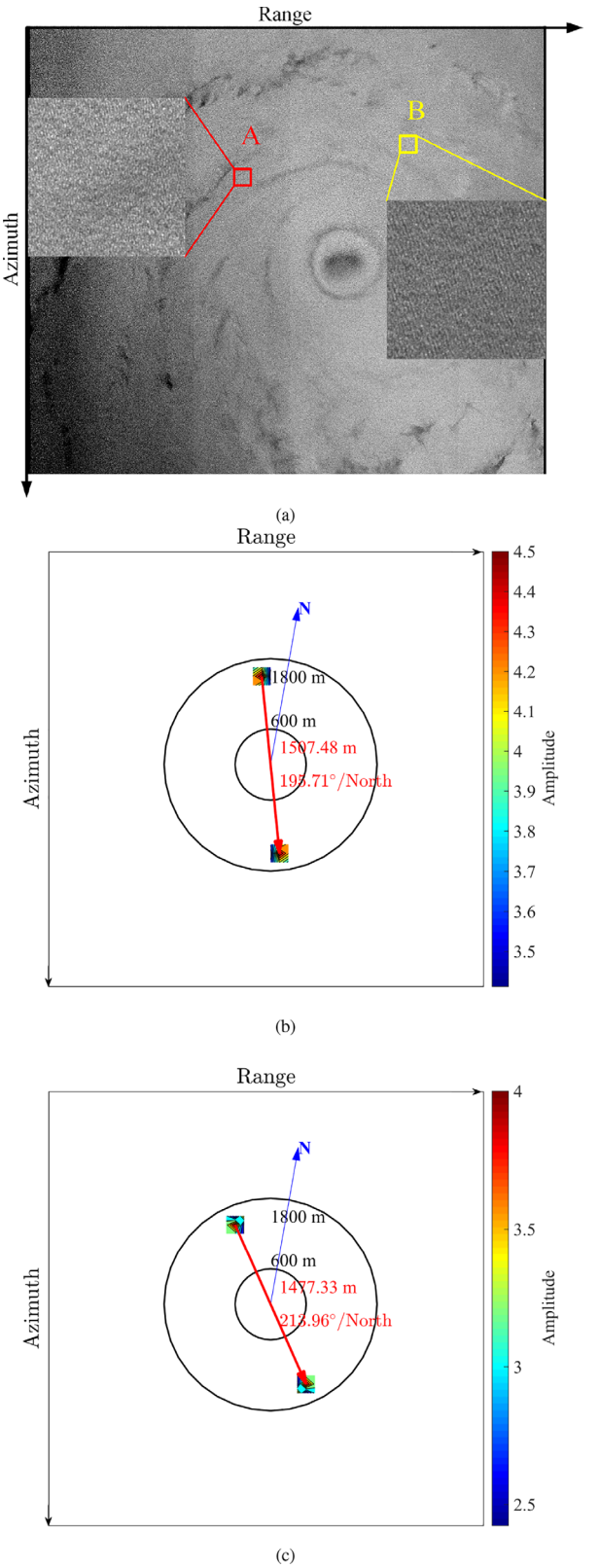

Figure 4. Extraction of roll characteristics. (a) SAR image of Hurricane Katrina 2005 acquired by ENVISAT. Subimages in Box A and B show the brush-like roll patterns. (b) 2D-FFT analysis of subimage in Box A. The dominant wavelength is about 1,507 m and orientation is about 196° (with 180° ambiguity). (c) 2D-FFT analysis of subimage in Box B. The dominant wavelength is about 1,477 m and orientation is about 214° (with 180° ambiguity).

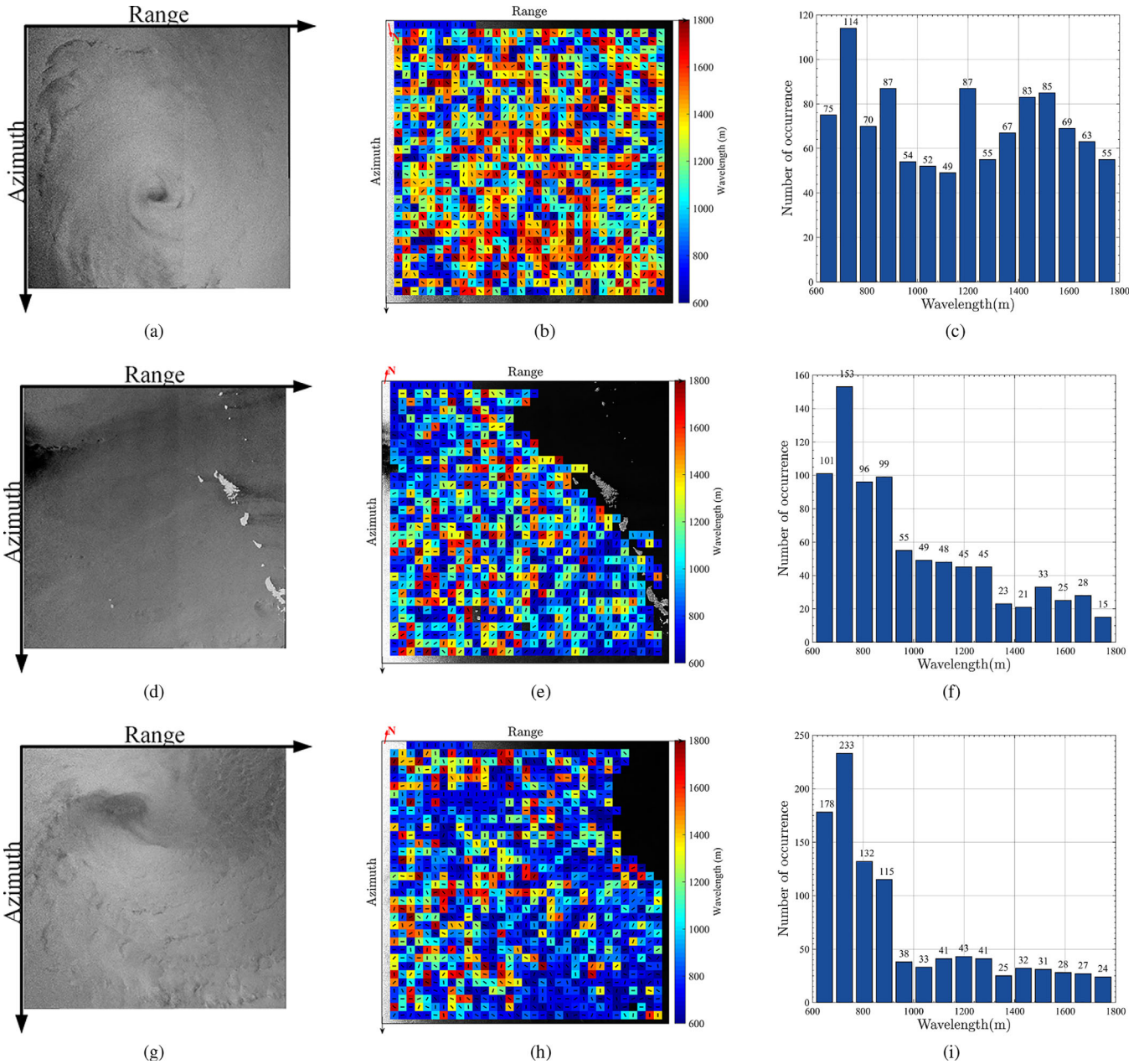

Figure 5. (a), (d), and (g) are SAR images of Hurricane Earl, Typhoon Fanapi, and Typhoon Malakas. (b), (e), and (h) are direction and wavelength of roll of Hurricane Earl, Typhoon Fanapi, and Typhoon Malakas. The colors present the wavelengths of rolls and the black lines indicate the directions (with 180° ambiguity) of rolls. (c), (f), and (i) are histograms of roll wavelengths Hurricane Earl, Typhoon Fanapi, and Typhoon Malakas.

In order to determine the roll wavelengths and directions from SAR images, a standard two-dimensional spectral analysis, which is widely used for roll extraction from SAR imagery (Lehner et al., 1998; Li et al., 2013a, 2013b; Reppucci et al., 2006; Zhang et al., 2008), is performed following four steps. First, the SAR images are calibrated. Second, the images are split into block subimages of 15×15 km. Third, a two-dimensional FFT (2D-FFT) is applied to each subimage. Finally, for each subimage, by finding the maximum for wavelength between 600 and 1,800 m, we determine the length and direction of the roll. Note that in the third step, in order to guarantee the quality of the derived roll characteristics, only the subimages above −22 dB are used for 2-D-FFT processing. The examples of 2-D-FFT analyses of Boxes A and B are shown in Figures 4b and 4c. The red arrows show the roll directions with 180° ambiguity, denoted as 196° and 214° relative to North, respectively. The wavelengths are calculated as 1,507 and 1,477 m, respectively. Note that in the northern hemisphere, since the TC's are counter clockwise rotation, the 180° ambiguity can be removed.

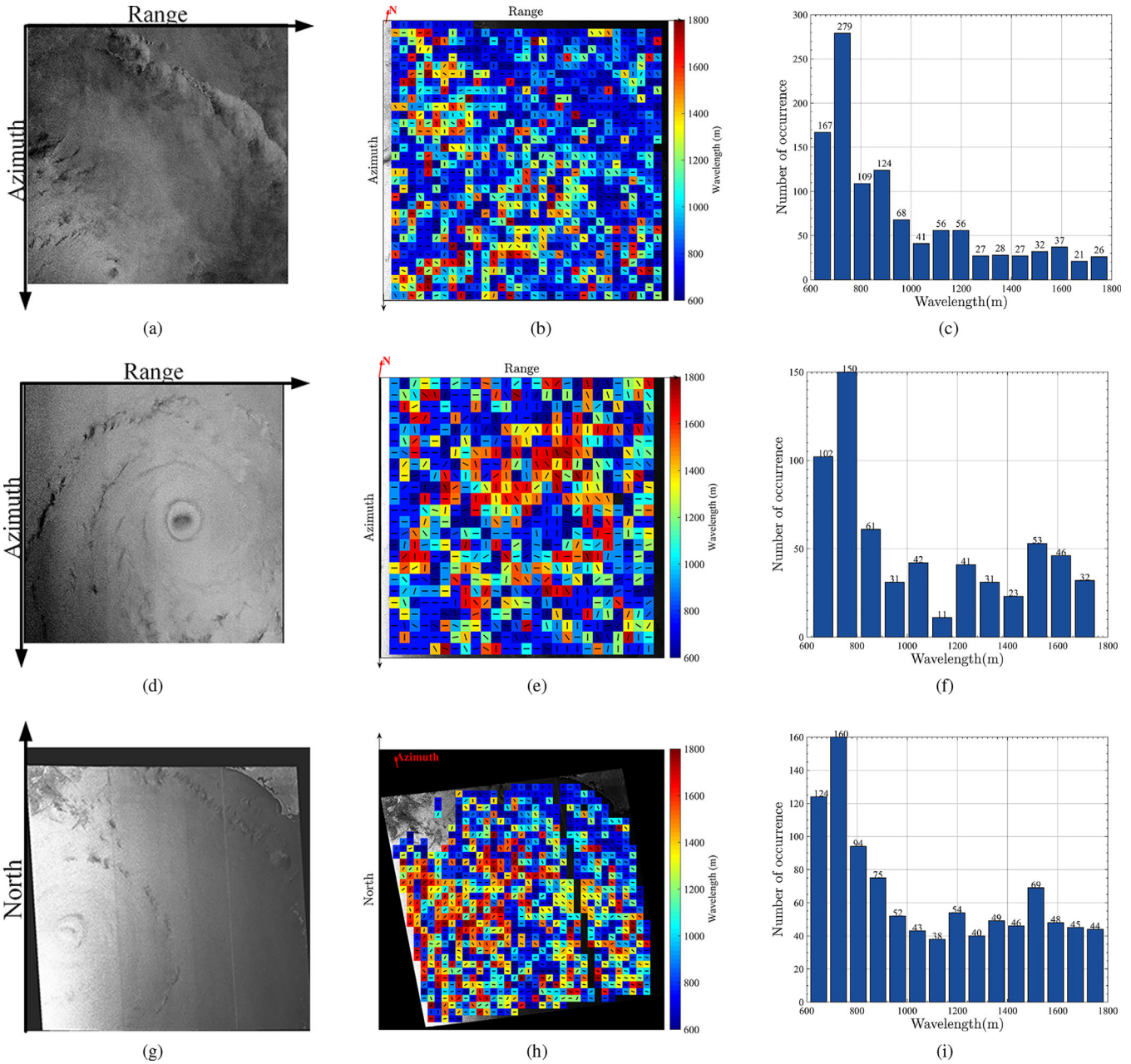

Figure 6. (a), (d), and (g) are SAR images of Typhoon Megi, Hurricane Katrina by ENVISAT, and Hurricane Katrina by RADARSAT-1. (b), (e), and (h) are direction and wavelength of roll of Typhoon Megi, Hurricane Katrina by ENVISAT, and Hurricane Katrina by RADARSAT-1. The colors present the wavelengths of rolls and the black lines indicate the directions (with 180° ambiguity) of rolls. (c), (f), and (i) are histograms of roll wavelengths Typhoon Megi, Hurricane Katrina by ENVISAT, and Hurricane Katrina by RADARSAT-1.

3. Results and Discussions

We extract roll wavelengths and directions for all TC's following the method presented in section 2.3. The histograms of the wavelengths of rolls across the whole SAR images are shown in Figures 5 and 6. For conciseness, the visual results of SENTINEL-1A data are not illustrated here.

From the second columns of Figures 5 and 6, different colors represent various wavelengths of rolls. For Hurricane Katrina (2005) (Figure 6d), our findings are in agreement with previous studies, showing the majority of wavelength of rolls are between 600 and 1, 600 m, which is consistent with previous study of Reppucci et al. (2006).

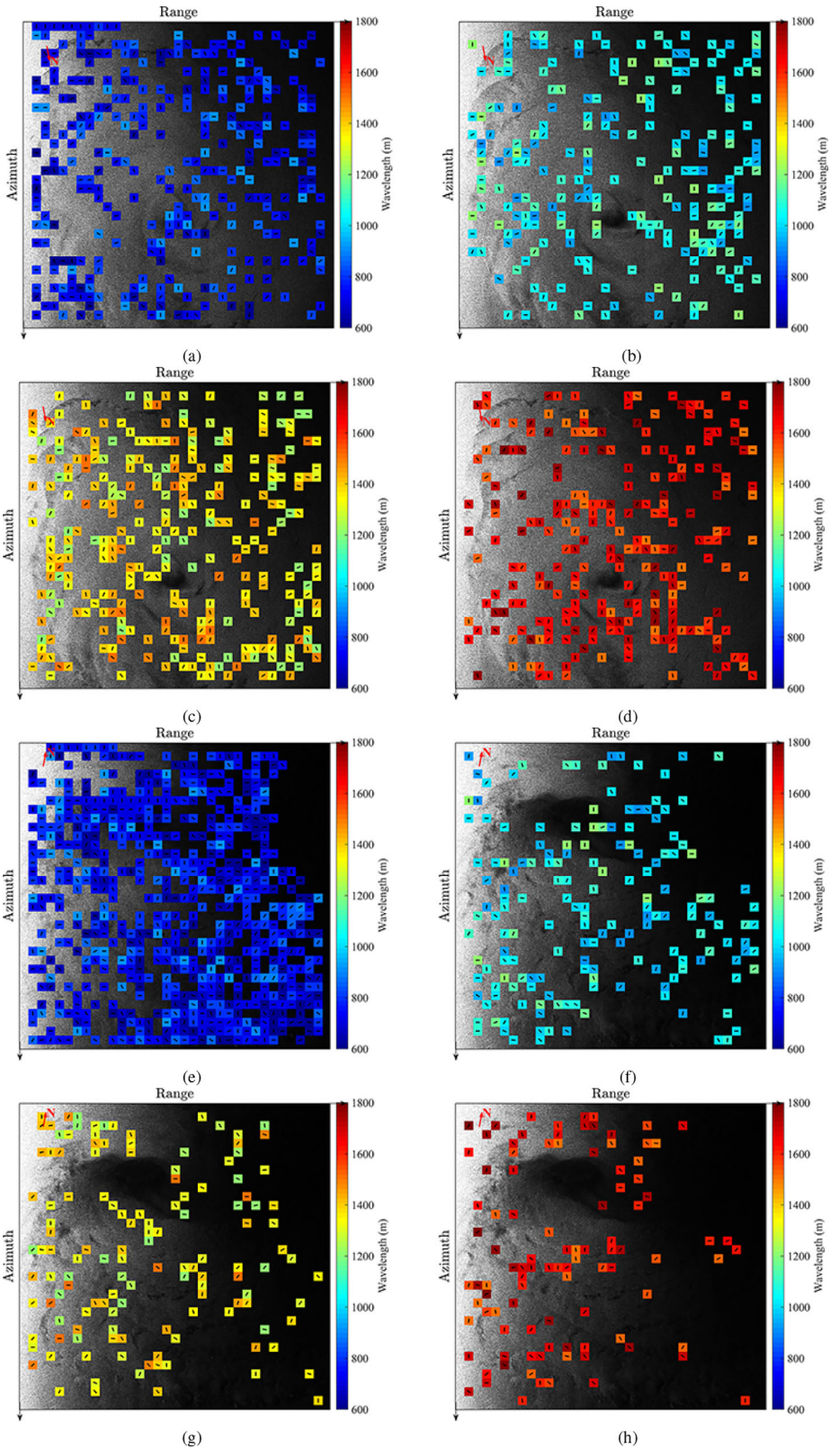

Figure 7. Spatial distributions of different ranges of roll wavelengths. The colors present the wavelengths of rolls and the black lines indicate the directions (with 180° ambiguity) of rolls. In the first and second rows, the subfigures are Hurricane Earl roll wavelengths between 600−900 m, 900−1,200 m, 1,200−1,500 m, and 1,500−1,800 m. In the third and fourth rows, the subfigures are Typhoon Malakas roll wavelengths between 600−900 m, 900−1,200 m, 1,200−1,500 m, and 1,500−1,800 m.

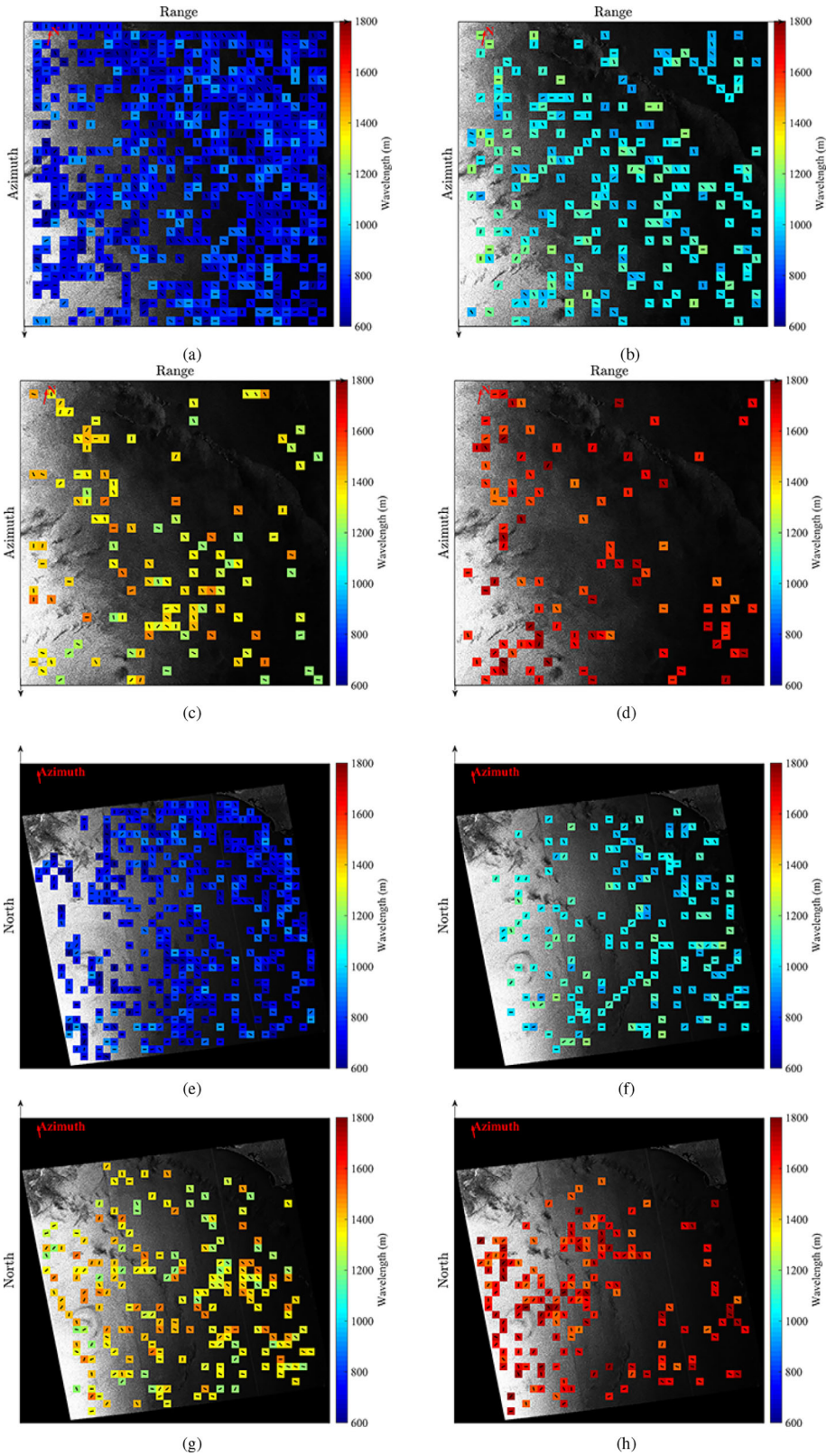

Figure 8. Spatial distributions of different ranges of roll wavelengths. The colors present the wavelengths of rolls and the black lines indicate the directions (with 180° ambiguity) of rolls. In the first and second rows, the subfigures are Typhoon Megi roll wavelengths between 600−900 m, 900−1, 200 m, 1, 200−1, 500 m, and 1, 500−1, 800 m. In the third and fourth rows, the sub-figures are Hurricane Katrina by RADARSAT-1 roll wavelengths between 600−900 m, 900−1, 200 m, 1, 200−1, 500 m, and 1, 500−1, 800 m.

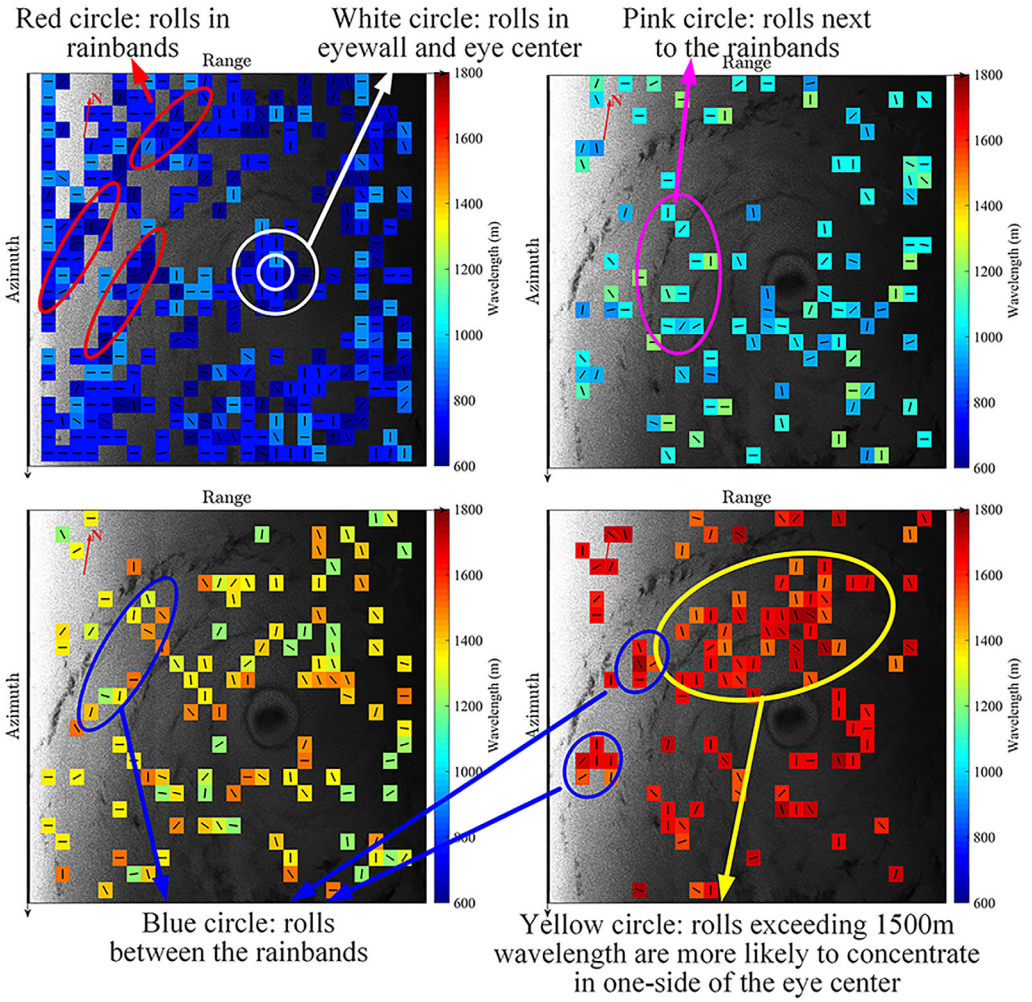

Figure 9. A detailed example of roll occurrence (Hurricane Katrina by ENVISAT). The colors present the wavelengths of rolls and the black lines indicate the directions (with 180° ambiguity) of rolls.

Furthermore, two observations are made. First, the roll wavelengths vary with the locations relative to the TC center. For example, in Figure 6e, it is evident that the roll wavelengths near the eye wall are smaller (represented in blue). Then the wavelengths become larger in some kilometers outside the area of eye core (represented in red). And with further locations relative to storm, the wavelengths tend to be smaller.

Second, the spatial distribution of roll wavelengths is asymmetrical. We take Hurricane Katrina (2005) as an example. It is obvious in Figure 6e, where the eye wall region is marked in yellow circle and the symmetrical axis is marked in black line. As we can see, the larger wavelengths tend to more concentrate on northwestern part (marked in pink circle) relative to the storm center.

In order to provide a deep understanding of these tentative observations, we elaborate the experimental results in both visual and quantitative ways, and give some analyses and discussion.

3.1. Occurrence of Rolls

In this subsection, we elaborate the occurrence of rolls. Two observations are made. First, we found that there exist roll imprints in eyewall and rainbands, although the MABL height may be shallower in these regions. Second, we observe that the spatial distribution of roll wavelengths is asymmetrical. For the five experimental data (Hurricane Earl, Typhoon Malakas, Typhoon Megi, Hurricane Katrina by ENVISAT, and Hurricane Katrina by RADARSAT-1), which captured the whole or part of eye structures, the spatial distributions of different ranges of roll wavelengths are shown in Figures 7–9. We divided the wavelengths into four intervals: $600-900$ m, $900-1,200$ m, $1,200-1,500$ m, and $1,500-1,800$ m. The SENTINEL-1 images are

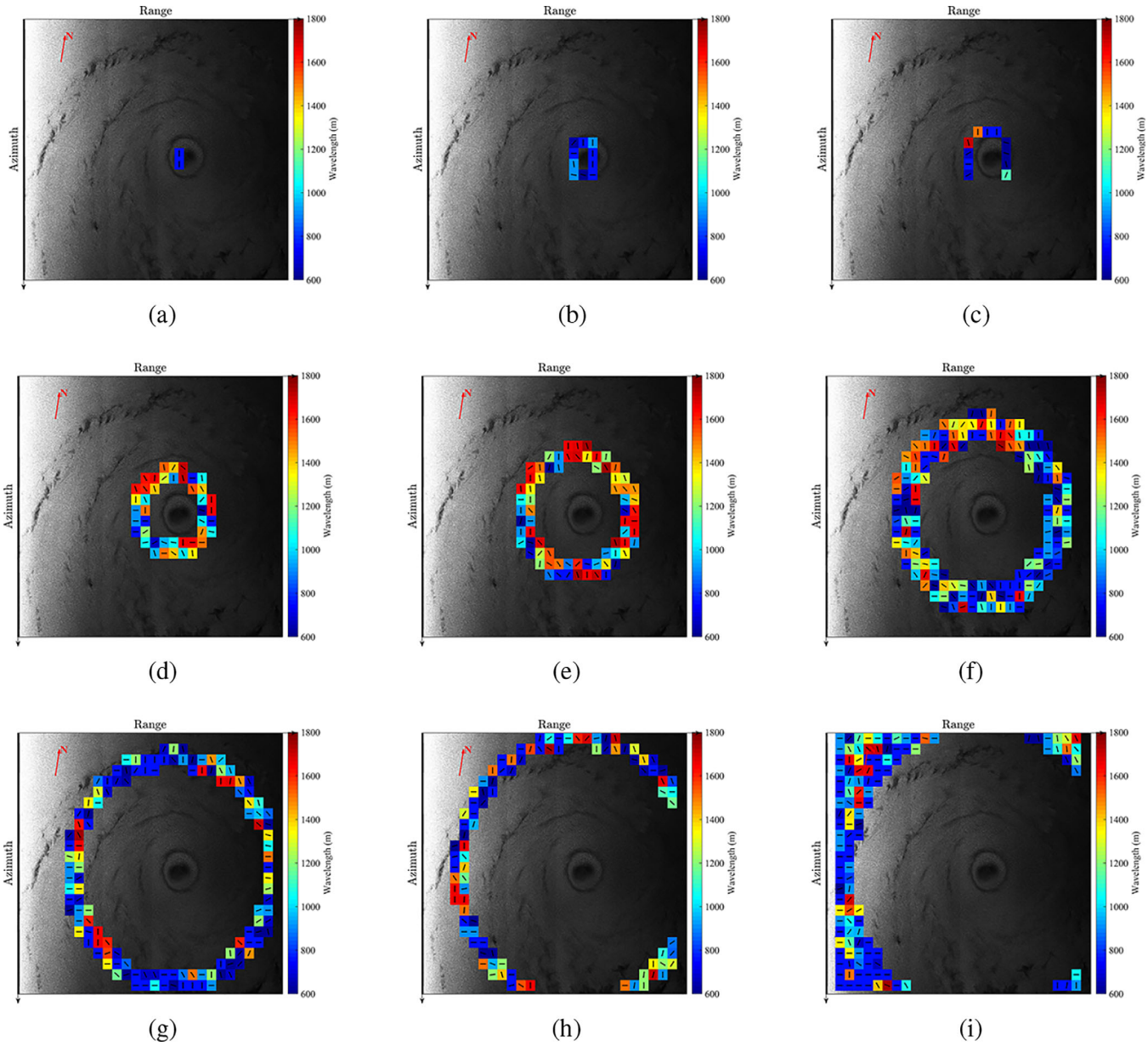

Figure 10. Roll wavelengths at different locations relative to the storm center of Hurricane Katrina acquired by ENVISAT. The colors present the wavelengths of rolls and the black lines indicate the directions (with 180° ambiguity) of rolls. (a) 0−15 km, (b) 15−30 km, (c) 30−40 km, (d) 40−70 km, (e) 70−100 km, (f) 100−145 km, (g) 145−175 km, (h) 175−200 km, and (i) >200 km.

not shown for conciseness. Since for Typhoon Fanapi, the image was captured further than 200 km distance away from the typhoon center, the experimental result of Fanapi is not discussed in this section.

First, we analyze the locations of rolls in different wavelength intervals. In order to be concise, we take Hurricane Katrina acquired by ENVISAT as an example (Figure 9). The rolls wavelengths under 900 m mostly locate at the eye center, eyewall, rainbands, or at distances larger than 200 km to hurricane center. Note that Foster (2005) demonstrated that rolls should be the expected basic state in TC regions outside the convective rainbands. Here, we found there still exist roll imprints in eyewall and rainbands, although the boundary layer height may be shallower in these regions. For the rolls whose wavelengths are between 900 and 1, 200 m, they are located next to rainbands or next to the eyewall. For the rolls with wavelengths between 1, 200 and 1, 500 m, they are mostly located out of the eyewall or between the rainbands. For the

rolls whose wavelengths exceed 1,500 m, many of them are concentrated in the location near to the outside regions of eyewall. The quantitative analyses of the locations will be given in section 3.2.

Besides, we observe that the spatial distribution of roll wavelengths is asymmetrical. Among the five SAR-imaged TC's, only the entire structures of Hurricane Earl and Hurricane Katrina are captured, the asymmetrical characteristic is relatively evident. In Figures 7d, 8h, and 9, the rolls with wavelength exceeding 1,500 m are more likely to concentrate in the upper part relative to storm center. This may due to the asymmetric convection and wind profiles within the TC's.

3.2. Roll Wavelengths Distribution With Respect to Storm Center

We define two locations relative to a TC center: the physical location and the normalized location. For one thing, the physical location is the true location relative to storm center. For simplicity, it will be referred as distance d in kilometer scale. For another, the normalized location relative to storm center is defined as the physical location normalized by the radius of maximum wind (RMW); that is, $d^* = d/\mathrm{RMW}$ (Zhang et al., 2013). Since RMW is one important characteristic of a storm (Zhang et al., 2013), this definition provides a reasonable comparison among various TC's. The wavelengths grouped as functions of d and d^* will be discussed, respectively.

First, based on the physical distance d, for each TC, the roll wavelengths at different locations relative to the storm center are calculated. An example of processing of Hurricane Katrina acquired by ENVISAT is given in Figure 10. Following the same processing, the measurements of all the TC's are summarized in Table 2. In generally, the roll wavelengths are relatively shorter around the hurricane center. With the increasing of d, the roll wavelengths become longer and reach the peak values at 30−175 km distance to TC centers. After reaching the peak values, the roll wavelength decrease with d.

Second, we exploit the rolls wavelength as a function of the normalized distance $d*$ to storm centers. RMW is estimated using the SAR retrieved wind speed detailed in section 2.2. The RMWs of Hurricane Earl and Typhoon Malakas are estimated as 59.5 and 128.5 km, respectively. The quantitative analyses are employed following the composite analysis method used by Zhang et al. (2011, 2013), which provides a general characterization of the structure. The data are composited through bin averaging with bin width of 0.5 for $d^* < 2$ and bin width of 1 for $d^* \geq 2$. Here, only the Hurricane Earl and Typhoon Malakas images, which have VH/HV data and captured TC centers, are discussed.

In Figure 11, the red line represents the values of mean wavelengths, and the blue line represents the values of mean wind speeds. We observe that rolls reach the peak wavelengths in the range of d^*-2d^*, a little further than RMW. One possible application is to estimate RMW by finding the radius with maximum wavelengths. This indicates the change of roll wavelength is slightly hysteretic compared to local wind speed. Besides, it can be visually observed that the roll wavelengths (red line) and the local wind speeds (blue line) present generally similar tendencies. The calculated correlation coefficients between them are illustrated in Figure 11. This demonstrates that roll characteristics are associated with the local wind speeds. Finally, we note that the wind speeds consistently decrease with d^*; whereas the roll wavelengths overall decrease with d^* but slightly fluctuate at larger d^*. This shows the complicated nature of roll characteristics. Further explanations are needed in the future work.

Table 2
Roll Wavelengths at Different Locations Relative to the Storm Centers

Name of TC\wave-length (m)\ distance (km)	0–15	15–30	30–40	40–70	70–100	100–145	145–175	175–200	>200
Earl	800	1,111	1,268	1,193	**1,340**	1,278	1,167	1,152	1,126
Fanapi									998
Malakas	705	787	732	909	991	1,026	**1,040**	919	920
Megi	767	1,042	1,042	**1,135**	1,097	984	972	993	922
Katrina-ENVISAT	750	773	890	1,248	**1,278**	1,038	968	1,052	972
Katrina-RADARSAT-1	1,270	1,236	1,028	1,238	**1,350**	1,216	1,114	1,072	1,013
Irma	909	1,003	**1,060**	947	857	899	864	843	926
Jose	1,207	1,202	**1,300**	1,263	1,250	1,256	1,250	1,182	1,195
Maria	1,050	1,089	1,155	1,241	1,260	1,388	**1,399**	1,269	1.017

Note. The bold texts indicate the maximum values of roll wavelengths and the locations where maximum wavelengths occur.

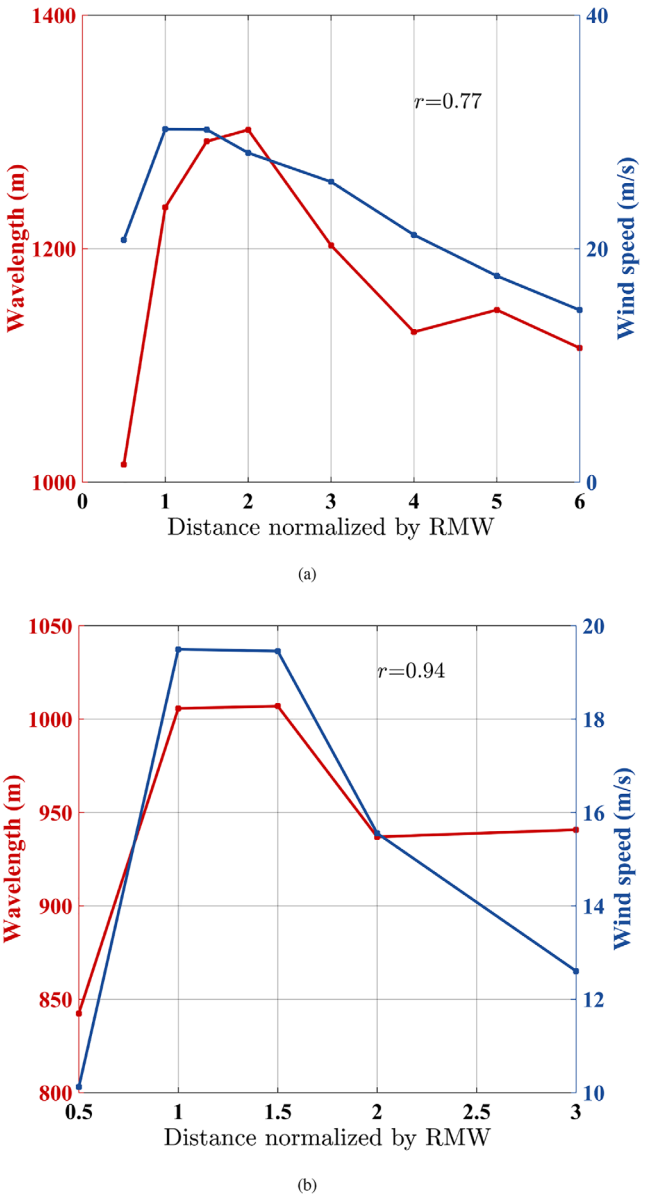

Figure 11. The wavelengths of rolls as a function of distance normalized by RMW. (a) Hurricane Earl and (b) Typhoon Malakas.

4. Conclusions

In this study, we calculated FFT algorithm to retrieve roll characteristics from SAR images. The experimental data set includes eight TC's and sixteen SAR images acquired by RADARSAT-1, RADARSAT-2, ENVISAT, and SENTINEL-1. By both visual and quantitative analyses, we investigate the variations of roll wavelengths associated with locations relative to the storm center. In summary, three observations are made.

First, we found there exists roll imprints in eyewall and rainbands, although the boundary layer height may be shallower in these regions.

Second, we observe that the spatial distribution of roll wavelengths is asymmetrical. The rolls with wavelength exceeding $1,500$ m are more likely to concentrate in the one-side part relative to storm center. This may due to that the storm structure is asymmetric such as convection and wind profiles.

Third, we quantitatively analyze the variances of roll wavelengths corresponding to both physical and normalized locations to storm centers. The roll wavelengths are relatively shorter around the hurricane center.

With the increasing of distances to storm center, the roll wavelengths become longer and reach the peak values. After reaching the peak values, the roll wavelength decrease with distances. In our study, rolls reach the peak wavelengths in the range of $d^* - 2d^*$. One possible application is to estimate RMW by finding the radius with maximum wavelengths.

This paper demonstrates the new capabilities to use SAR data for MABL roll research. SAR allows us to systematically map the distribution and wavelength of MABL rolls under different-scale hurricane conditions for the first time. This work aims at answering the question how roll characteristics vary with locations to storm center. Furthermore, since rolls are closely related to hurricane dynamics, we also expect this work to be promising to bring roll-induced effects into hurricane forecasting model. The future work involves more theoretical explanation of these observations by dropsonde data in the composite study. Furthermore, how roll characteristics vary with storm intensities will be investigated.

Acknowledgments

The authors would like to thank the Canadian Space Agency for providing RADARSAT-1/2 data, the European Space Agency for providing the ENVISAT data, and the SENTINEL-1 data. We thank anonymous reviewers for comments that improved the paper. The Radarsat-1/2 and Envisat SAR images are provided by Canadian Space Agency and European Space Agency, respectively. The Sentinel-1 SAR images are available via Copernicus Open Access Hub (https://scihub.copernicus.eu/dhus/#/home). The auxiliary data used in this paper such as the SFMR data and the best track data can be downloaded via NOAA http://www.aoml.noaa.gov/hrd/data_sub/sfmr.html and http://www.nhc.noaa.gov/data/#hurdat, respectively. The views, opinions, and findings contained in this paper are those of the authors and should not be construed as an official NOAA or U.S. government position, policy, or decision.

References

Foster, R. C. (2005). Why rolls are prevalent in the hurricane boundary layer. *Journal of the Atmospheric Sciences*, *62*(8), 2647–2661.

Friedman, K., & Li, X. (2000). Storm patterns over the ocean with wide swath SAR. *Johns Hopkins University Applied Physics Lab Technical Digest*, *21*(1), 80–85.

Gao, K., Ginis, I., Doyle, J. D., & Jin, Y. (2017). Effect of boundary layer roll vortices on the development of an axisymmetric tropical cyclone. *Journal of the Atmospheric Sciences*, *74*(9), 2737–2759.

Goldenberg, S. B., Landsea, C. W., Mestas-Nuñez, A. M., & Gray, W. M. (2001). The recent increase in Atlantic hurricane activity: Causes and implications. *Science*, *293*(5529), 474–479.

Hwang, P. A., Zhang, B., Toporkov, J. V., & Perrie, W. (2010). Comparison of composite Bragg theory and quad-polarization radar backscatter from RADARSAT-2: With applications to wave breaking and high wind retrieval. *Journal of Geophysical Research*, *115*, C08019. https://doi.org/10.1029/2009JC005995

Jin, S., Wang, S., & Li, X. (2014). Typhoon eye extraction with an automatic SAR image segmentation method. *International Journal of Remote Sensing*, *35*(11–12), 3978–3993. https://doi.org/10.1080/01431161.2014.916447

Jin, S., Wang, S., Li, X., Jiao, L., Zhang, J. A., & Shen, D. (2017). A salient region detection and pattern matching-based algorithm for center detection of a partially covered tropical cyclone in a SAR image. *IEEE Transactions on Geoscience and Remote Sensing*, *55*(1), 280–291. https://doi.org/10.1109/TGRS.2016.2605766

Katsaros, K. B., Vachon, P. W., Black, P. G., Dodge, P. P., & Uhlhorn, E. W. (2000). Wind fields from SAR: Could they improve our understanding of storm dynamics? *Johns Hopkins APL Technical Digest*, *21*(1), 86–93.

Katsaros, K. B., Vachon, P. W., Liu, W. T., & Black, P. G. (2002). Microwave remote sensing of tropical cyclones from space. *Journal of Oceanography*, *58*(1), 137–151.

Lee, I. K., Shamsoddini, A., Li, X., Trinder, J. C., & Li, Z. (2016). Extracting hurricane eye morphology from spaceborne SAR images using morphological analysis. *ISPRS Journal of Photogrammetry and Remote Sensing*, *117*, 115–125. https://doi.org/10.1016/j.isprsjprs.2016.03.020

Lehner, S., Horstmann, J., Koch, W., & Rosenthal, W. (1998). Mesoscale wind measurements using recalibrated ERS SAR images. *Journal of Geophysical Research*, *103*(C4), 7847–7856.

Li, X. (2015). The first Sentinel-1 SAR image of a typhoon. *Acta Oceanologica Sinica*, *34*(1), 1–2. https://doi.org/10.1007/s13131-015-0589-8

Li, X., Pichel, W. G., He, M., Wu, S. Y., Friedman, K. S., Clemente-Colón, P., et al. (2002). Observation of hurricane-generated ocean swell refraction at the Gulf Stream north wall with the RADARSAT-1 synthetic aperture radar. *IEEE Transactions on Geoscience and Remote Sensing*, *40*(10), 2131–2142. https://doi.org/10.1109/TGRS.2002.802474

Li, X., Zhang, J. A., Yang, X., Pichel, W. G., DeMaria, M., Long, D., et al. (2013a). Tropical cyclone morphology from spaceborne synthetic aperture radar. *Bulletin of the American Meteorological Society*, *94*(2), 215–230. https://doi.org/10.1175/BAMS-D-11-00211.1

Li, X., Zheng, W., Yang, X., Zhang, J. A., Pichel, W. G., & Li, Z. (2013b). Coexistence of atmospheric gravity waves and boundary layer rolls observed by SAR. *Journal of the Atmospheric Sciences*, *70*(11), 3448–3459.

Lorsolo, S., Schroeder, J. L., Dodge, P., & Marks, F. Jr. (2008). An observational study of hurricane boundary layer small-scale coherent structures. *Monthly Weather Review*, *136*(8), 2871–2893.

Morrison, I., Businger, S., Marks, F., Dodge, P., & Businger, J. A. (2005). An observational case for the prevalence of roll vortices in the hurricane boundary layer. *Journal of the Atmospheric Sciences*, *62*(8), 2662–2673.

Overland, J. E., & Wilson, J. G. (1984). Mesoscale variability in marine winds at mid-latitude. *Journal of Geophysical Research*, *89*(C6), 10,599–10,614.

Pielke, R. A. Jr., & Landsea, C. W. (1998). Normalized hurricane damages in the United States: 1925–95. *Weather and Forecasting*, *13*(3), 621–631.

Reppucci, A., Lehner, S., & Schulz-Stellenfleth, J. (2006). Tropical cyclone parameters derived from synthetic aperture radar (SAR) images In *IEEE International Conference on Geoscience and Remote Sensing Symposium, 2006. IGARSS 2006* (pp. 2220–2223). Piscataway, NJ: IEEE.

Shao, W., Li, X., Hwang, P., Zhang, B., & Yang, X. (2017). Bridging the gap between cyclone wind and wave by C-band SAR measurements. *Journal of Geophysical Research: Oceans*, *122*, 6714–6724. https://doi.org/10.1002/2017JC012908

Shen, H., Perrie, W., He, Y., & Liu, G. (2014). Wind speed retrieval from VH dual-polarization RADARSAT-2 SAR images. *IEEE Transactions on Geoscience and Remote Sensing*, *52*(9), 5820–5826.

Svensson, N., Sahlée, E., Bergström, H., Nilsson, E., Badger, M., & Rutgersson, A. (2017). A case study of offshore advection of boundary layer rolls over a stably stratified sea surface. *Advances in Meteorology*, 2017, 9015891. https://doi.org/10.1155/2017/9015891

Wikipedia, the free encyclopedia (2017). *2017 Atlantic hurricane season*. Retrieved from https://en.wikipedia.org/wiki/2017_Atlantic_hurricane_season.

Wurman, J., & Winslow, J. (1998). Intense sub-kilometer-scale boundary layer rolls observed in Hurricane Fran. *Science*, *280*(5363), 555–557.

Zhang, B., Perrie, W., Vachon, P. W., Li, X., Pichel, W. G., Guo, J., et al. (2012). Ocean vector winds retrieval from C-band fully polarimetric SAR measurements. *IEEE Transactions on Geoscience and Remote Sensing*, *50*(11), 4252–4261.

Zhang, G., Li, X., Perrie, W., Hwang, P. A., Zhang, B., & Yang, X. (2017a). A hurricane wind speed retrieval model for C-band RADARSAT-2 cross-polarization scansar images. *IEEE Transactions on Geoscience and Remote Sensing*, *55*(8), 4766–4774. https://doi.org/10.1109/TGRS.2017.2699622

Zhang, G., Perrie, W., Li, X., & Zhang, J. A. (2017b). A hurricane morphology and sea surface wind vector estimation model based on C-band cross-polarization SAR imagery. *IEEE Transactions on Geoscience and Remote Sensing*, *55*(3), 1743–1751. https://doi.org/10.1109/TGRS.2016.2631663

Zhang, J. A., Katsaros, K. B., Black, P. G., Lehner, S., French, J. R., & Drennan, W. M. (2008). Effects of roll vortices on turbulent fluxes in the hurricane boundary layer. *Boundary-Layer Meteorology*, *128*(2), 173–189.

Zhang, J. A., & Li, X. (2017). Tropical cyclone multiscale wind features from spaceborne synthetic aperture radar. In X. Li (Ed.), *Hurricane monitoring with spaceborne synthetic aperture radar* (Chap. 2, pp. 25–37). Berlin, Germany: Springer.

Zhang, J. A., Rogers, R. F., Nolan, D. S., & Marks, F. D. Jr. (2011). On the characteristic height scales of the hurricane boundary layer. *Monthly Weather Review*, *139*(8), 2523–2535.

Zhang, J. A., Rogers, R. F., Reasor, P. D., Uhlhorn, E. W., & Marks, F. D. Jr. (2013). Asymmetric hurricane boundary layer structure from dropsonde composites in relation to the environmental vertical wind shear. *Monthly Weather Review*, *141*(11), 3968–3984.

Zheng, G., Yang, J., Liu, A. K., Li, X., Pichel, W. G., & He, S. (2016). Comparison of typhoon centers from SAR and IR images and those from best track data sets. *IEEE Transactions on Geoscience and Remote Sensing*, *54*(2), 1000–1012. https://doi.org/10.1109/TGRS.2015.2472282

Zhou, X., Yang, X., Li, Z., Yu, Y., Bi, H., Ma, S., et al. (2013). Estimation of tropical cyclone parameters and wind fields from SAR images. *Science China Earth Sciences*, *56*(11), 1977–1987. https://doi.org/10.1007/s11430-013-4633-2